Indian Journal of Radio & Space Physics
Vol 45, March 2016, pp 11-19

Detection of ionospheric spatial and temporal gradients for ground based augmentation system applications

Swapna Raghunath[1,$] & D Venkata Ratnam[2,#,*]

[1]Dept of ECE, G Narayanamma Institute of Technology and Science, Hyderabad 500 008, India

[2]Dept of ECE, Koneru Lakshmaiah University, Guntur 522 502, India

E-mail: [$]swapna_raghunath@rediffmail.com; [#]dvratnam@kluniversity.in

Received 25 October 2015; revised 18 January 2016; accepted 12 February 2016

Standalone Global Navigation Satellite System (GNSS) is inadequate for precise navigation of aircrafts. Ground-based Augmentation System (GBAS) augments the performance of GNSS for civil aviation by providing differential corrections to the position of an aircraft during takeoff and landing. Ionospheric gradients affect the accuracy of GNSS and they can be detected and characterized from GNSS observations. In this paper, the ionospheric temporal and spatial gradients have been detected and the ionospheric drift velocity has been evaluated from the data recorded by GNSS receivers located at Koneru Lakshmaiah University, Guntur (GNT) and Indian Meteorological Department, Machilipatnam (MPM), Andhra Pradesh, India. Both the stations are chosen as they are situated close to each other and to the Vijayawada Airport. The rate of TEC index (ROTI) and numerical differentiation are applied to detect the ionospheric temporal gradients. Time-step and Station-pair methods are used to detect the spatial gradients. Ionospheric gradients at GNT and MPM stations for the month of January 2015 have been discussed. The gradients are found to have occurred mostly between 2000 and 2200 hrs LT. The maximum value of ionospheric gradient velocity is 473.25 ms^{-1}. The S4 value is above 0.8 and the phase scintillation value is above 0.7 radians.

Keywords: Ionospheric drift velocity, Ground-based Augmentation System (GBAS), Ionospheric gradient, Ionospheric pierce point, Total electron content

PACS Nos: *94.20.dv*; 94.80.+g; 84.40.Ua

1 Introduction

Ground Based Augmentation System (GBAS) is becoming indispensable in airports as it is relatively inexpensive, physically compact, self contained and easy to deploy. GBAS works in conjunction with the satellite-based navigation system to provide very precise navigation service, which in turn ensures increased safety as compared to standalone satellite navigation. International Civil Aviation Organization (ICAO) has proposed to replace the current Instrumental Landing System (ILS) with GBAS in the long term due to better performance at lower installation, maintenance and lifecycle costs[1]. The architecture of a GBAS system is illustrated in Fig. 1.

GBAS is composed of satellite constellation, ground station and the aircraft receiver. The GBAS ground station consists of three or four reference receivers at exactly pre-calculated locations, a GBAS ground facility and a very high frequency (VHF) data broadcast (VDB) transmitter. The reference receivers get the positioning data from GNSS satellites and relay the information, regarding pseudo-range measurements, signal health and system performance, to the GBAS central processing facility. GBAS ground facility computes the corrections using GNSS data from reference receivers and transmits the integrity information to the aircraft receiver *via* a VDB signal over a frequency band of 108 - 117.975 MHz (Ref. 1).

The aircraft receiver receives the positioning information from the GNSS satellites as well as the differential corrections from the GBAS ground station. The aircraft receiver applies the differential corrections on the GNSS data to produce a set of corrected pseudo-ranges. GBAS is capable of providing corrections to most of the GNSS pseudo-range errors that the aircraft experiences in and around an airport. During disturbance period, the behaviour of ionosphere shows strong temporal and spatial variations. In the equatorial or low latitude regions (within 20°N or S), the commonly observed ionospheric disturbances are large gradients in total electron content (TEC), plasma bubbles, scintillations,

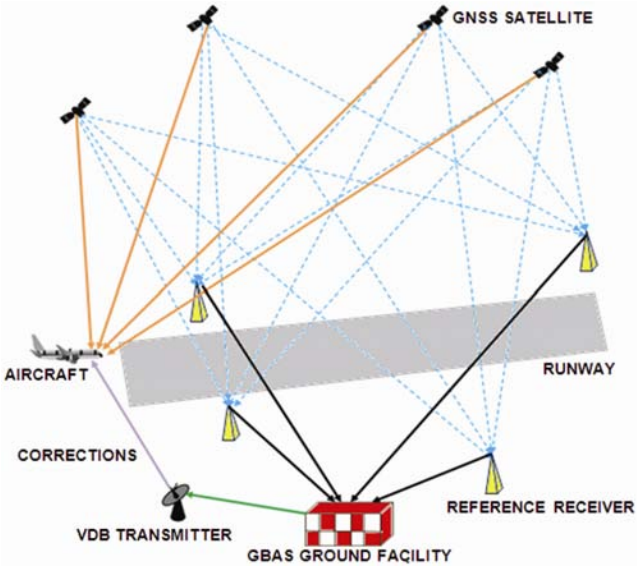

Fig. 1 — GBAS architecture

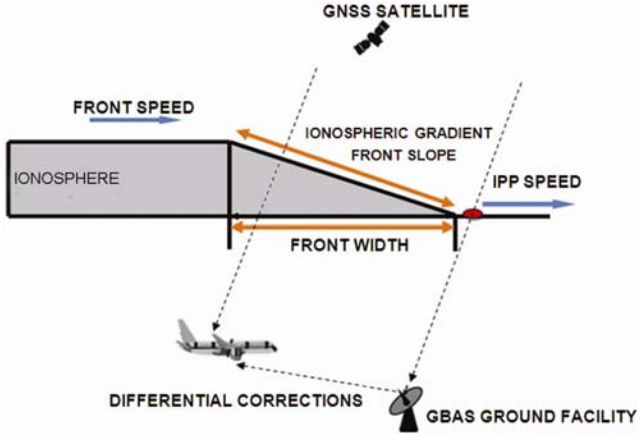

Fig. 2 — Ionospheric threat model for GBAS

equatorial fountain and sub-equatorial anomalies. This anomalous behaviour results in ionospheric threat almost all the time, especially during the post sunset hours. Since the ionospheric threat consists of moving ionospheric wave fronts, the threat model is formulated considering the three important parameters, viz. slope, velocity and width of the ionospheric front. In this paper, the characteristics of ionospheric gradients that travelled over the low latitude regions of the Indian subcontinent have been evaluated. Positioning information is collected using the NovAtel, GPStation-6 receivers at Koneru Lakshmaiah University, Guntur (GNT) and Indian Meteorological Department, Machilipatnam (MPM), Andhra Pradesh. The temporal gradients in the ionosphere are detected using the front velocity of the ionospheric threat model for GBAS. Figure 2 depicts that the delay in the range experienced by the aircraft is different from the delay experienced by the GBAS ground facility.

Spatial gradients are found at the GNT and MPM stations. The amplitude and phase scintillation values are studied and they indicated strong ionospheric disturbance during the post sunset hours, which coincided with the usual time of occurrence of the spatial and temporal gradients in low latitudes[2]. TEC is a key parameter in detecting as well as mitigating the errors due to anomalous behaviour of ionosphere. The velocity of the ionospheric front can be calculated from the slant total electron content (STEC) values recorded by the two GPS stations. The drift velocity of a plasma bubble in the low latitude regions can be found by finding the cross covariance and auto covariance of the TEC values from two geographically close GNSS stations and measuring the time lag in the observed disturbance at the two places[3].

The detection of medium scale disturbances in the ionosphere over mid-latitudes can be done by Statistical Angle-of-Arrival and Doppler Method (SADM-GPS)[4]. SADM-GPS computes the velocity of TEC gradient using data from 3 GPS stations. The noise is removed by time averaging the velocity measurements. Short period disturbances of 3 - 10 minutes can be detected using discrete time cross correlation between normalized data from pairs of GPS stations[5]. The propagation velocity of ionospheric disturbance is computed by simplified geometry. The drift velocity of equatorial ionospheric scintillations can be estimated using cross correlation between STEC observations of local GPS reference network[6-8]. The spatial and temporal gradients in the ionosphere affect only a few satellites that pass over the disturbance. The present work focuses on detecting the presence of ionospheric disturbance and also determining the satellite vehicles, which are affected by the same. Avoiding the affected satellites mitigates the error introduced in the GNSS signal due to the variation in ionospheric delay between the user and the ground facility[9].

2 Data and Analysis

GPS data is recorded using NovAtel GPStation-6 GNSS Ionospheric Scintillation and TEC Monitor (GISTM) receivers at Koneru Lakshmaiah University (16.4415°N; 80.62179°E), Guntur (GNT) and Indian Meteorological Department (16.08°N; 81.15°E),

Machilipatnam (MPM), near Vijayawada Airport (16.31°N; 80.47°E), Andhra Pradesh, India, to detect and determine the characteristics of the ionospheric gradient. The distance between the two stations is 56.79 km. The distances from Vijayawada Airport to GNT and MPM stations are 22 and 77 km, respectively. According to the specifications provided by the Federal Aviation Administration, GBAS provides navigation and precision approach service over a radius of 23 nautical miles around the host airport. Usually, the TEC values are calibrated to remove TEC biases from the measured TEC. The biases in TEC measurements may occur due to GNSS antenna, antenna cable, connectors, splitters, amplifiers, working temperature and equipment ageing. NovAtel GPStation-6 receiver has an inbuilt auto calibration feature for determination of instrumental biases. The instrumental biases, thus, determined are included in the TEC measurements automatically by GPStation6 receiver.

The STEC variations with respect to local time are extracted from the GPS data recorded over the month of January 2015. The data is collected at intervals of 60 seconds. The ionospheric gradients are detected and their velocities are evaluated.

2.1 Auto detection of ionospheric gradients in GNSS radio signals

In this paper, automatic detection of ionospheric temporal gradients has been done using rate of TEC index (ROTI) and numerical differentiation methods.

2.1.1 Rate of TEC index (ROTI)

TEC fluctuations are usually characterized by the standard deviation of TEC (σ_{STEC}). The rate of TEC index is the standard deviation of rate of change of TEC (ROT) as shown in Eq. (1). ROTI is a better tool than σ_{STEC} as taking the derivative of TEC while calculating ROTI automatically removes the unknown TEC biases and background trends and emphasizes the high frequency components of TEC fluctuations. ROTI is the standard deviation of ROT as given by Eq. (2). $STEC(i)$ and $STEC(i-1)$ are the STEC values measured at the current instant 'i' and the previous instant 'i-1', respectively.

$$ROT(i) = STEC(i) - STEC(i-1) \quad \ldots (1)$$

$$ROTI = \sqrt{\frac{\sum_{i=1}^{N}(ROT(i) - \overline{ROT})^2}{N}} \quad \ldots (2)$$

where, N, is the number of samples or epochs. In this paper, ROTI values have been evaluated over a sliding window of size of 10 min (N = 10). The maxima of all ROTI values indicate the occurrence of a gradient. ROTI is a very popular ionospheric gradient detection techniques due to the simplicity of its evaluation but it suffers from the drawback that its value has a strong dependence on the size of the window or the number of epochs over which it is evaluated, the latitude of the GNSS receiver and the sample rate or the time interval between two consecutive epochs. The sample rate is an important parameter when small scale structures of plasma are to be detected, whereas the window size is very important while detecting large scale plasma structures. Jacobsen[10] showed that when the size of the plasma structure is unknown, ROTI is not a very accurate detection technique. In this paper, the window size for ROTI calculation is taken as 10 minutes and the time interval between two epochs is 1 minute. Another simple yet effective ionospheric plasma irregularity detection technique is the numerical differentiation method.

2.1.2 Numerical differentiation

Numerical differentiation method of detecting ionospheric gradient overcomes the disadvantages of ROTI. The main trends of STEC, which are the high amplitude and low frequency components, appear due to the diurnal cycle of the Sun and the continuous change in the navigational satellite geometry with respect to a GNSS receiver. Numerical derivative of STEC completely removes the main trend and the disturbance period can be highlighted[11]. The first order derivative of STEC, $\delta STEC$ for the *i*th sample is given by Eq. (3):

$$\delta STEC(i) = STEC(i) - \frac{STEC(i-1)+STEC(i+1)}{2} \quad \ldots (3)$$

After performing the first order derivative, the disturbance can be observed as the high amplitude signals. To verify if the remaining low amplitude signals are disturbance or just noise, a second order derivative, $\delta\delta STEC$ is computed in a similar way as shown in Eq. (4).

$$\delta\delta STEC(i) = \delta STEC(i) - \frac{\delta STEC(i-1)+\delta STEC(i+1)}{2} \quad \ldots (4)$$

The time at the highest value of $\delta\delta STEC$ gives the instant of occurrence of a gradient.

2.2 Shifting of STEC and Separating the disturbance period

GNT and MPM stations are less than 60 km apart and TEC values observed by both from a common

satellite should be almost the same but their receiver hardware biases could be different, which may introduce errors in the velocity calculations. In order to eliminate the difference in receiver biases, the STEC values of GNT are shifted by the mean of the difference in STEC values of the two stations, $dSTEC$ as given in Eqs (5) and (6):

$$dSTEC = STEC(GNT) - STEC(MPM) \quad \ldots (5)$$

$$Shifted\ STEC = STEC(GNT) - \overline{dSTEC} \quad \ldots (6)$$

In order find the drift velocity of the ionospheric gradient, the covariance of the STEC values during the disturbance period is evaluated.

2.3 Cross covariance and Auto covariance calculation

The ionospheric gradient has a measurable velocity. When the gradient is traversing in the ionosphere and exhibiting temporal changes, then, its velocity can be calculated by Eq. (7):

$$V = \frac{\Delta D}{\Delta t} \quad \ldots (7)$$

where, ΔD, is the geographical distance between the two stations (GNT and MPM). The time lag between the maxima of the cross covariance of GNT and MPM and the auto covariance of GNT gives Δt. The equations for cross covariance and auto covariance are given by Eqs (8 and 9):

$$C_{pq} = \frac{\sum_{i=1}^{n}(p_i-\bar{p})(q_i-\bar{q})}{n} \quad \ldots (8)$$

$$C_{pp} = \frac{\sum_{i=1}^{n}(p_i-\bar{p})(p_{i+1}-\bar{p})}{n} \quad \ldots (9)$$

where, p_i and q_i, are the ith samples of STEC values of GNT and MPM stations and $\bar{p}$ and $\bar{q}$ are their mean values, respectively.

2.4 Ionospheric spatial gradient

Ionosphere extends from approximately 70 to 1000 km from the surface of the earth. The ionospheric thin shell model assumes the ionosphere to be a thin shell of uniform density at a constant height of 350 km from the surface of the earth where the electron density is maximum. In order to find the ionospheric spatial gradients, the ionospheric pierce points (IPP) must be calculated. IPP is the point of intersection of a GNSS signal from the satellite to the receiver with the ionosphere at a height of 350 km (H_{IPP}) from the surface of the earth. The latitude and longitude of IPP, φ_{IPP} and λ_{IPP}, respectively are given by Eqs (10 and 11):

$$\varphi_{IPP} = sin^{-1}(sin\varphi_g cos\mathcal{R}_{PP} + cos\varphi_g sin\mathcal{R}_{PP} cosaz) \quad \ldots (10)$$

$$\lambda_{IPP} = \lambda_g + sin^{-1}\left(\frac{sin\mathcal{R}_{PP} sinaz}{cos\varphi_{IPP}}\right) \quad \ldots (11)$$

where,

$$\mathcal{R}_{PP} = {}^{\pi}/_{2} - el - sin^{-1}\left(\frac{R_e cosel}{R_e + H_{IPP}}\right) \quad (12)$$

where, φ_g and λ_g, are the latitude and longitude of the ground station receiver; az and el, the azimuth and elevation angle in radians of the satellite in question as seen from the receiver; R_e the radius of the earth; and H_{IPP}, the height of the ionospheric thin shell[12].

Ionospheric spatial gradient, which is the variation of STEC over space, can be computed by two methods, viz. Time-step method and Station-pair method[13]. In Time-step method, the difference in the ionospheric delay at two consecutive epochs is computed for one station and the result is divided with the distance between the IPPs at the two instants. The spatial gradient computed by the Time-step method has an inherent temporal component in it, which makes it not so accurate for GBAS applications.

In Station-pair method, the gradient is found by computing the ionospheric delay difference between two closely spaced stations, in the view of a common satellite, at a particular epoch and dividing it with the distance between the IPPs of the two stations at the same time instant. The expressions for spatial gradients computed using Time-step method and Station-pair method are given by Eqs (13 and 14):

$$Spatial\ Gradient_{Time-Step} = \frac{STEC(i+1) - STEC(i)}{DIPP_i} \quad \ldots (13)$$

$DIPP_i$ = distance between IPPs corresponding to time instants i and i+1.

$$Spatial\ Gradient_{Station-Pair} = \frac{STEC(Rx1) - STEC(Rx2)}{DIPP_{Rx12}} \ldots (14)$$

$DIPP_{Rx12}$ = distance between IPPs of two stations at the same instant.

3 Results and Discussion

The STEC values recorded at the GPS stations at GNT and MPM over the month of January 2015 have been processed to detect ionospheric spatial and temporal gradients. GPS signals at low elevation angles have to travel longer distances than those at high elevation angles resulting in a greater path loss. Signals at low elevation angles are also corrupted by multipath propagation due to obstacles in their path. Therefore, only elevation angles above 30 degrees

have been considered while calculating all the ionospheric parameters.

For demonstration, the data on 9 January 2015 for PRN 3 has been considered. The 9 January 2015 was a geomagnetically quiet day with Kp index of 2. The STEC values at the two stations are shown in Fig. 3. The variations in the STEC values in Fig. 3 indicate turbulence in the ionosphere from 2000 to 2030 hrs LT. A maximum STEC value of 42.58 TECU is recorded at GNT station and a maximum value of 41.20 TECU was recorded at MPM station.

The auto detection of ionospheric gradient can be done by calculating the ROTI values using Eqs (2 and 3). Here, ROTI values of GNT and MPM stations have been evaluated using a sliding window of 10 minutes duration as shown in Fig. 4. The maximum value of ROTI indicates the presence of a gradient. Figure 4 shows that ROTI values of GNT and MPM are high between 2000 and 2100 hrs LT. GNT has a maximum ROTI value of 0.9983 TECU/min at 2045 hrs LT and MPM has a maximum value of 1.6868 TECU/min at 2028 hrs LT.

The first order and second order numerical differentials of the STEC values of GNT and MPM stations on 9 January 2015 for PRN 3 are calculated using Eqs (4) and (5), respectively. The first order differential is shown in Fig. 5 and the second order differential is shown in Fig. 6. The large variations in the first order differentials of GNT and MPM indicate a disturbance in the interval 2000 - 2030 hrs LT. The high values of the second order differential during the same time interval reinforces the conclusion made from Figs 4 and 5.

The difference in the STEC values of GNT and MPM according to Eq. (6) is shown in Fig. 7. After the presence of ionospheric gradient is detected, the STEC plot of GNT is shifted to the mean value of MPM in order to remove the difference in the receiver biases using Eqs (6 and 7) (Ref. 3) as shown in Fig. 8.

In order to calculate the velocity of the gradient with a higher accuracy, STEC values during the period of disturbance only are considered. The STEC values during the disturbance period from 2018 to 2030 hrs LT are shown in Fig. 9.

The cross-covariance of STEC values of GNT and MPM and the auto covariance of STEC values of

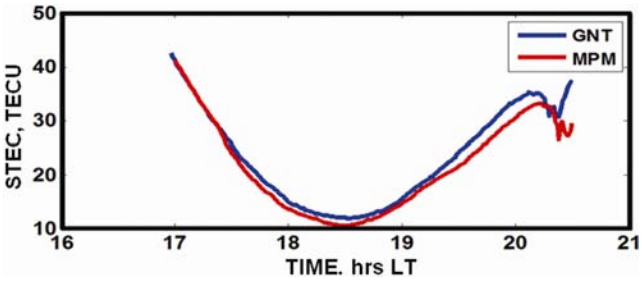

Fig. 3 — STEC values observed at the two GPS Stations on 9 January 2015 for PRN 3

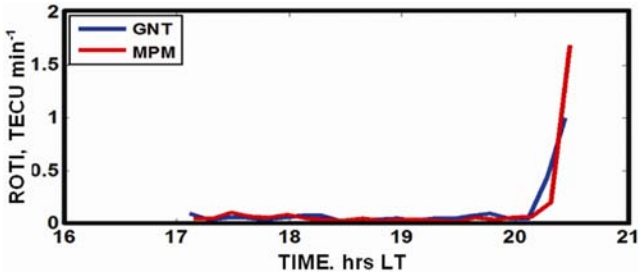

Fig. 4 — ROTI values for KLU Station on 9 January 2015 for PRN 3

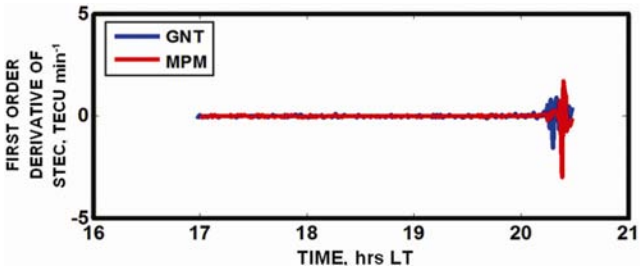

Fig. 5 — First order differential of STEC measured at GNT on 9 January 2015 for PRN 3

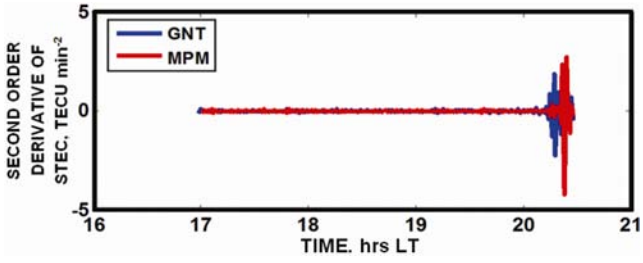

Fig. 6 — Second order differential of STEC measured at GNT on 9 January 2015 for PRN 3

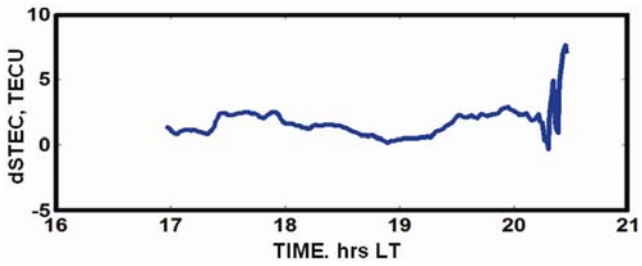

Fig. 7 — Difference between STEC values of GNT and MPM on 9 January 2015 for PRN 3

GNT are calculated using Eqs (9) and (10), respectively. The cross covariance and auto covariance are shown in Fig. 10. The auto covariance of STEC values during the disturbance period at GNT station has a maximum at sample number 9 and the cross covariance of the STEC values of GNT and MPM station, during the disturbance period between 2018 and 2100 hrs LT, has a maximum at sample number 14 as shown in Fig. 10. The samples are taken at intervals of 60 seconds. The time lag between the cross covariance of GNT and MPM and the auto covariance of GNT is found to be 300 s. The distance between GNT and MPM is 56.79 km, which gives the velocity of the gradient as 189.3 ms^{-1} using Eq. 8.

The IPP latitudes and longitudes are calculated using Eqs (10 - 12). The spatial gradients using the Time-Step method is computed from Eq. (13) for both GNT and MPM stations and the same are depicted in Fig. 11. The IPP distance between consecutive epochs for the two stations lies between 3.2 and 7.7 km. The spatial gradient is found to have an average value of

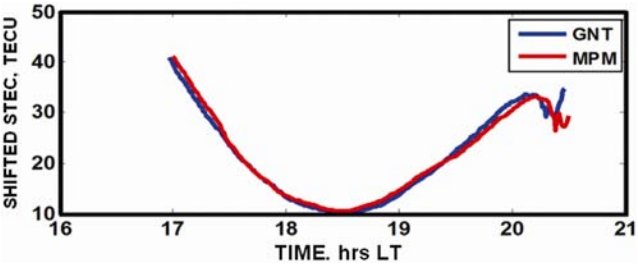

Fig. 8 — Shifted STEC on 9 January 2015 for PRN 3

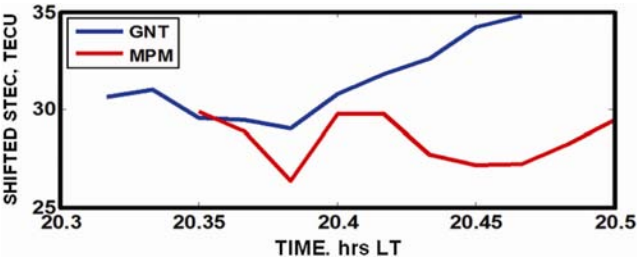

Fig. 9 — STEC values during the disturbance period on 9 January 2015 for PRN 3

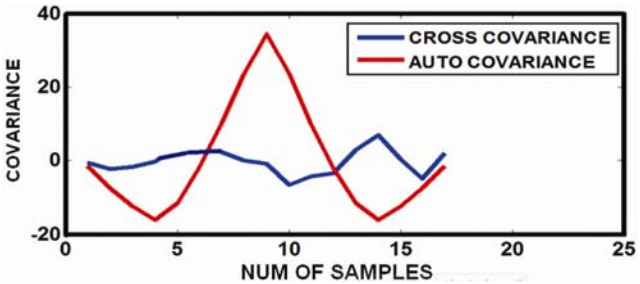

Fig. 10 — Covariance of STEC values at GNT and MPM during disturbed period on 9 January 2015 for PRN 3

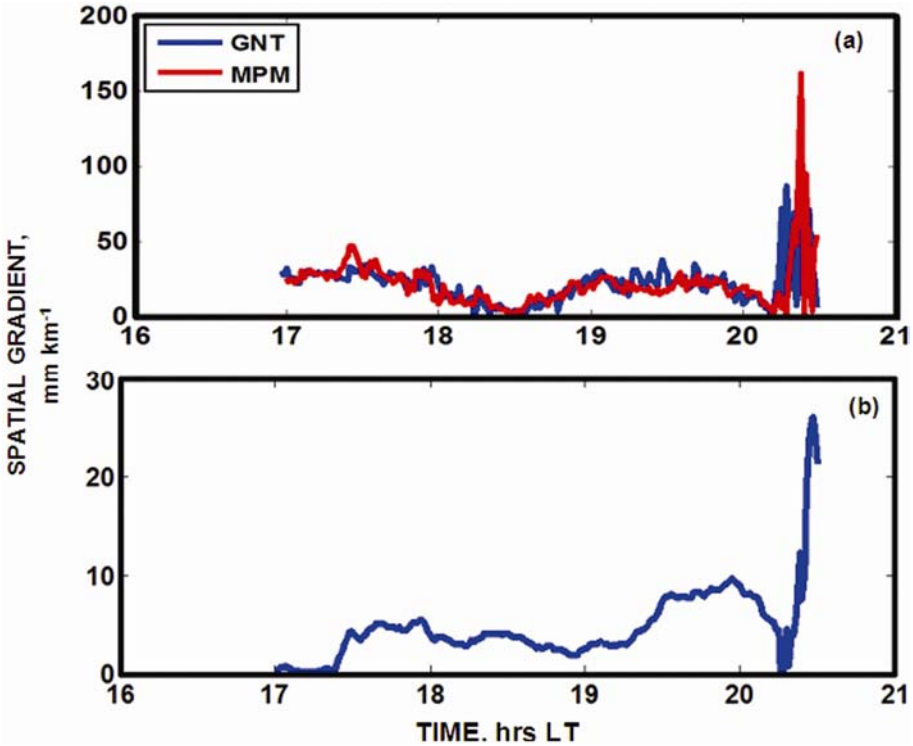

Fig. 11 — Spatial gradients for GNT and MPM on 9 January 2015 for PRN 3 using: (a) Time-step method; and (b) Station-pair Method

22 mm km^{-1} over the entire day on 9 January 2015 for PRN 3 but during the disturbance period, it reaches a maximum value of 86.6 mm km^{-1} at 2028 hrs LT over GNT and 161.4 mm km^{-1} at 2038 hrs LT over MPM. The high values of spatial gradients between 2000 and 2030 hrs LT coincide with the time of occurrence of temporal gradients as seen in Fig. 3.

The spatial gradients from Station-pair method are shown in Fig. 12. The distance between the IPPs corresponding to the two stations lies in the range 53.71 - 59.67 km. The maximum value of the spatial gradient is found to be 25.04 mm km^{-1} at 2028 hrs LT.

Ionospheric disturbances can also be detected by observing the amplitude scintillation (S4) and phase scintillation. When a radio signal from a GNSS satellite passes through a disturbed ionosphere, it undergoes rapid fluctuations in amplitude and phase due to the dispersive nature of the medium. These fluctuations are called scintillations and they indicate the amount of inconsistency in the radio signal. An S4 value of greater than 0.6 and likewise a phase scintillation value of 0.5 and above indicate strong disturbance[14]. Figure 12 shows the S4 and phase scintillation on 9 January 2015 for PRN 3. The maximum value of S4 recorded at GNT 0.726 at 2029 hrs LT. At MPM, the maximum value of S4 is recorded as 0.83 at 2036 hrs LT. The maximum values of phase scintillation during the disturbance period at GNT and MPM are recorded to be 0.65 radians at 2027 hrs LT and 0.71 radians at 2035 hrs LT, respectively. The high values of S4 and phase scintillation indicate strong scintillation, which occurred as a result of the spatial and temporal gradients. Figure 13 shows that the spatial gradient calculated by the Time-step method at GNT has a maximum value of 102.4 mm km^{-1} for PRN 23 and at MPM, it is 129 mm km^{-1} for PRN 9. The Station-pair method used to measure the spatial gradients as seen at both GNT and MPM stations simultaneously and it had a maximum value of 35.27 mm km^{-1} for PRN 23.

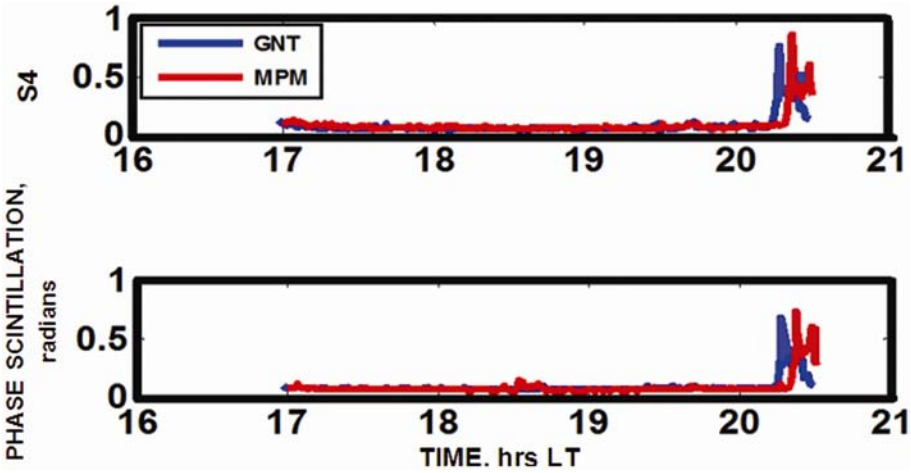

Fig. 12 — S4 and phase scintillation on 9 January 2015 for PRN 3

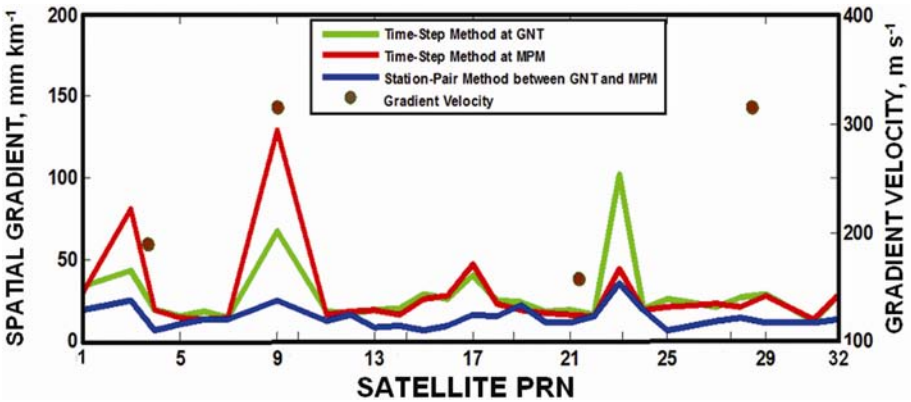

Fig. 13 — Spatial gradient values evaluated using Time-step and Station-pair methods and velocities of the gradients

Table 1 — Summary of the ionospheric gradients for January 2015 at GNT and MPM stations

Date	PRN	STEC, TECU		ROTI, TECU		Time, hrs LT (hh:mm)	Velocity, ms^{-1}	Spatial gradient, mm km^{-1}			S4		Phase scintillation, radians	
								Time-Step		Station-Pair				
		GNT	MPM	GNT	MPM			GNT	MPM	GNT-MPM	GNT	MPM	GNT	MPM
08 Jan 2015	14	53.34	51.31	0.15	0.11	11:30 – 15:00	315.5	31.32	29.04	8.90	0.15	0.15	0.08	0.24
09 Jan 2015	3	42.5	41.2	0.99	1.68	19:00	189.3	43.31	80.74	25.04	0.43	0.11	0.4	0.14
09 Jan 2015	9	25.60	20.69	1.33	1.72	22:48	315.5	66.75	129.0	24.72	0.22	0.11	0.20	0.14
09 Jan 2015	23	31.56	25.54	2.28	0.87	22:30	157.7	102.4	43.96	35.27	0.63	0.11	0.30	0.14
09 Jan 2015	31	59.44	63.68	0.08	0.08	13:45	315.5	12.04	13.42	11.56	0.08	0.11	0.10	0.14
10 Jan 2015	21	55.28	53.27	2.04	1.19	12:00-13:00	473.2	224.8	176.48	12.71	0.62	0.87	0.48	0.24
11 Jan 2015	31	55.98	59.35	0.09	0.09	14:30 – 15:00	157.7	119.6	50.52	13.83	0.09	0.11	0.10	0.16
14 Jan 2015	21	58.34	55.02	0.11	2.7	9:12 – 10:00	118.3	229.6	183.42	14.41	0.13	0.15	0.13	0.16
18 Jan 2015	28	39	34.85	0.96	2.44	21:30 – 22:30	126.8	134.3	192.77	56.37	0.44	0.58	0.41	0.48
19 Jan 2015	11	16.55	12.23	1.31	0.69	21:30 – 23:30	105.1	75.21	84.54	21.04	0.19	0.13	0.15	0.14
20 Jan 2015	28	35.37	34.54	6.52	4.17	21:30 – 23:00	189.3	348.2	297.46	66.82	0.85	0.72	0.62	0.5
21 Jan 2015	9	22.02	20.56	2.82	2.21	20:30 – 21:30	157.7	95.76	98.04	50.77	0.29	0.38	0.24	0.47
22 Jan 2015	9	32.53	33.67	3.63	7.53	21:00 – 22:00	236.6	138.5	169.7	50.74	0.54	0.58	0.58	0.5
25 Jan 2015	9	28.41	27.12	3.61	1.03	21:00 – 22:00	315.5	136.1	112.24	42.25	0.45	0.37	0.46	0.19
26 Jan 2015	9	54.58	53.47	2.17	4.36	21:00 – 22:00	294.6	217.6	240.01	44.07	0.49	0.54	0.54	0.18
27 Jan 2015	19	47.42	41.19	4.73	2.6	20:00 – 21:12	289.3	223.4	227.97	62.42	0.79	0.49	0.46	0.88

Only PRNs 3, 9, 23 and 31 were affected by the ionospheric gradients on 9 January 2015. The gradient velocities measured for these PRNs are shown in Fig. 13. A maximum value of 315.5 mm km^{-1} is found at PRN 9.

A summary of the affected satellites and the maximum values of the important parameters, namely STEC, ROTI, spatial gradients, S4 and phase scintillation along with the duration of the disturbance is detailed in Table 1. Only the satellites signals, which pass through disturbance, are affected. The velocity of the gradient varied from 105.16 to 473.25 m s^{-1}. The S4 and the phase scintillation had a maximum value of 0.878 and 0.65 radians, respectively in January 2015. The disturbance period was predominantly in the post sunset hours between 2000 and 2200 hrs LT, which is the usual behaviour of ionosphere in the low latitudes[6].

4 Conclusion

GBAS systems improve positioning accuracy in civil aviation by providing differential corrections to the GNSS data. Out of the various errors that a GNSS signal encounters, ionospheric error is the most difficult to mitigate. In this study, an attempt has been made to detect the spatial and temporal gradients in the ionosphere in the low-latitude regions at the Guntur (GNT) and Machilipatnam (MPM) stations over the month of January 2015. ROTI and numerical differentiation techniques were used to detect the gradients and the velocity of the gradient was computed using covariance of the STEC values. The IPPs were calculated, which were used to find the ionospheric spatial gradients. The amplitude and phase scintillations were also observed. The spatial and temporal gradients and the scintillation values indicated a strong ionospheric disturbance between 2000 and 2100 hrs LT. The methodology used in this study is simple, yet effective in evaluating the characteristics of ionospheric gradients. This study can be furthered by measuring the resulting Doppler shifts to establish exact direction of the ionospheric gradient and proposing corrections to the aircraft receiver during the disturbance period.

Acknowledgement

One of the authors (DVR) would like to express his thanks to the Department of Science and Technology, New Delhi, India for funding this research through the SR/S4/AS-91/2012 and SR/FST/ESI-130/2013(C) FIST program. Thanks are due to the anonymous reviewers for their valuable comments for improving the quality of this paper

References

1 Murphy T & Imrich T, Implementation and operational use of Ground-Based Augmentation Systems (GBASs) — A component of the future air traffic management system, Proc *IEEE (USA),* 96 (12) (2008) pp 1936-1957.

2 Raghunath S & Ratnam D V, Detection of low-latitude ionospheric irregularities from GNSS observations, *IEEE J Sel Topics Appl Earth Obs Remote Sens (USA),* 8 (11) pp 5171-5176.

3 Bumrungkit A, Rungraengwajiake S, Supnithi P & Saekow A, Analysis of ionospheric irregularity observed near Suvarnabhumi International Airport in Thailand, *Appl Mechanics Mater (Germany)*, 781 (2015) pp 85-88.

4 Afraimovich E L, Perevalova N P & Voyeiko S V, Traveling wave packets of total electron content disturbances as deduced from global GPS network data, *J Atmos Sol-Terr Phys (UK)*, 65 (2003) pp 1245-1262.

5 Garrison J L, Lee S G, Haase J S & Calais E, A method for detecting ionospheric disturbances and estimating their propagation speed and direction using a large GPS network, *Radio Sci (USA)*, 42 (6) (2007) pp 47-65.

6 Ji S, Chen W, Ding X & Zhao C, Equatorial ionospheric zonal drift by monitoring local GPS reference networks, *J Geophys Res (USA),* 116 (A8) (2011) pp 13-27.

7 Mayer C, Belabbas B, Jakowski N, Meurer M & Dunkel W, Ionosphere threat space model assessment for GBAS, *Proceedings of the 22nd International Technical Meeting of The Satellite Division of the Institute of Navigation* (ION GNSS 2009), *(*Institute of Navigation*,* Savannah, GA), 2009, pp 1091-1099.

8 Hofmann W B, Lichtenegger H & Collins J, *GPS theory and practice* (Springer, New York), 2001, 212.

9 Ravi Chandra K, Satya Srinivas V & Sarma A D, Investigation of ionospheric gradients for GAGAN application, *Earth, Planet Space (Japan)*, 61 (2009) pp 633–635.

10 Jacobsen K S, The impact of different sampling rates and calculation time intervals on ROTI values, *J Space Weath Space Clim (France)*, 4 (A33) (2014) pp 1-9.

11 Park J, *Ionospheric monitoring by the Global Navigation Satellite System*, PhD Thesis, Geodetic Science and Surveying, The Ohio State University, 2012.

12 Sunehra D, Validation of GPS receiver instrumental bias results for precise navigation, *Indian J Radio Space Phys*, 42 (2013) pp 175-181.

13 Jiyun L, Sam P, Datta-Barua S & Per E, Assessment of ionosphere spatial de-correlation for global positioning system-based aircraft landing systems, *J Aircraft (USA)*, 44 (5) (2007) pp 1662-1669.

14 Smita D, Rashmi W, Ekkaphon M & Gwal A K, Study of *amplitude and phase scintillation* at GPS frequency, *Indian J Radio Space Phys*, 34 (2005) pp 402-407.